encit 2020

ABCM Associação Brasileira de Engenharia e Ciências Mecânicas

18th Brazilian Congress of Thermal Sciences and Engineering
November 16–20, 2020 (Online)

ENC-2020-0060
THE AHMED BODY'S EXTERNAL AERODYNAMICS AT 25° SLANT ANGLE REAR SURFACE: A NUMERICAL ANALYSIS USING CFD

Jorge Esteban Chavez Gutierrez
jorge.chavez@labmci.ufsc.br
Mechanical Engineering - Francisco de Paula Santander University - IM/FI/UFPS.
Avenida Gran Colombia No. 12E-96 Barrio Colsag, San José de Cúcuta, NS, Colombia.
Internal Combustion Engines Laboratory - Joinville Technological Center - Federal University of Santa Catarina - LABMCI/CTJ/UFSC.
Rua Dona Francisca 8300, Joinville, SC, CEP 89219-600, Brazil.

Luis Emilio Vera Duarte
luisemiliovd@ufps.edu.co
Mechanical Engineering - Francisco de Paula Santander University - IM/FI/UFPS.
Avenida Gran Colombia No. 12E-96 Barrio Colsag, San José de Cúcuta, NS, Colombia.

Amir Antonio Martins Oliveira Jr.
amir.oliveira@gmail.com
Combustion and Thermal Systems Engineering Laboratory - Mechanical Engineering - Federal University of Santa Catarina - LABCET/EMC/CTC/UFSC,.
Bairro Trindade, Florianópolis, SC, CEP 88040-900, Brazil.

Leonel R Cancino
leonel.cancino@labmci.ufsc.br
Internal Combustion Engines Laboratory - Joinville Technological Center - Federal University of Santa Catarina - LABMCI/CTJ/UFSC.
Rua Dona Francisca 8300, Joinville, SC, CEP 89219-600, Brazil.

Abstract. *In this work, a numerical computational fluid dynamics approach of the field flow around the Ahmed's body reference geometry was performed. The main target was to analyze the external aerodynamics looking at the main relevant aspects as vortex generation, velocity and pressure fields, fluid separation and reattachment as well as the drag and lift contributions of each surfaces in the body. Domain and mesh independence tests were performed in order to numerically warrant no influence on the results. Four turbulence models were used in order to better elucidate the numerical effect of the turbulence model in the results. Experimental data from literature was then used to assess the numerical procedures adopted along this work as well as to identify the turbulence model that better fits the experimental results in terms of drag and lift forces. Numerical results shows that the realizable κ - ε turbulence model well approximates the drag with 3.9% difference to experimental results and the Reynolds Stress Model better fits the lift with 2.8% difference to experimental results.*

Keywords: *Ahmed's body reference geometry, Computational fluid dynamics, Road vehicle aerodynamics, Drag and lift forces, Turbulence models*

1. INTRODUCTION - THE AHMED BODY REFERENCE GEOMETRY FOR EXTERNAL AERODYNAMICS RESEARCH

Greenhouse gas emissions (GHG) coming from combustion process of internal combustion engines in ground vehicles have strong impact in the climate change. Alternatives have been sought to reduce and improve the overall energetic efficiency of road vehicles using, for example: (a) materials of high resistance and low weight, (b) reducing the aerodynamic drag designing streamlines vehicle's geometries, and (c) the use of hybrid engines and / or alternative fuels for energy improving (Agarwal, 2013). Vehicle aerodynamics has been developed in order to determine the relationship between the air flow around (and through) the flow field. The air flow that passes through the engine and compartments (internal flow) is completely dependent on the flow around the vehicle (external flow). The external flow generates forces and moments on the vehicle, which determine the car's performance and directional stability. Another purpose of vehicle aerodynamics is to avoid water and dirt on the windows and the surface of the lights, additionally, to minimize any aero acoustic effect

that can rise because the movement of the car. On the other hand, to provide the air flow for the cooling of the engine and passengers compartment, among other functions (Stone and Ball, 2004). Additionally, the energy delivered by the fuel is not 100% used, about 50% of the available mechanical energy is used to overcome the vehicle's aerodynamic drag at high speeds. The aerodynamic drag is composed by pressure drag and friction drag. The first is generated by the vehicle front and rear pressure difference, and the friction drag is generated by the surface air shear stress. The aerodynamic drag is greatly influenced by the vehicle external geometry (shape) and the size of the cross-sectional area, moreover it increases quadratically with the speed of the vehicle. Consequently, by decreasing the drag of the vehicle it is possible to make better use of the energy delivered by the fuel (Agarwal, 2013). Computational techniques as computational fluid dynamics (CFD) are used to assess the aerodynamic performance of a vehicle in relation to drag, lift, moments, pressure center, among others. Another great advantage of CFD is that the results are obtained in a relatively short time. This allows to simulate potential real-life scenarios in which a vehicle can be found, allowing to clearly understand and analyze the interaction between the vehicle and the surrounding air (Ahmed *et al.*, 1984). The objective of this study is to analyze through CFD tools, the external aerodynamics of the Ahmed' body reference geometry. This geometry greatly represents the vortices and the airflow generated around a real vehicle. Different aerodynamic performance can be found according to the angle of the inclined surface at the rear of Ahmed's body reference geometry. For the development of this study was selected the angle of 25° in the rear inclined surface, which represents the vortices that are generated in a fastback-type vehicle. With the objective of finding data congruent with reality, in this study emphasis was placed on guaranteeing that the results were independent of both, the number of mesh elements and the computational domain length. Additionally, different sizes of control volumes were included to guarantee the refinement of elements around the geometry. At the same time, taking advantage of this CFD tool, other simulations were carried out with different turbulence models, such as the κ - ε, which has shown results in the range of 2% to 5% compared to results found in experiments performed in wind tunnels. Subsequently the numerical results obtained in the simulations are exhaustively analyzed and compared to experimental data found in the literature obtained from wind tunnel measurements.

2. METHODOLOGY

The Ahmed's body reference geometry is composed by three parts: the front section, which is rounded to keep the flow attached to the surface; the central section, represented by a rectangular box with sharp edges; and the back inclined surface, where the flow shows different behaviors, according to the angle of inclination (Guilmineau, 2018). Figure 1 and Table 1 shows the geometry's shape and main dimensions for slant angle of 25.0°, focus of this work.

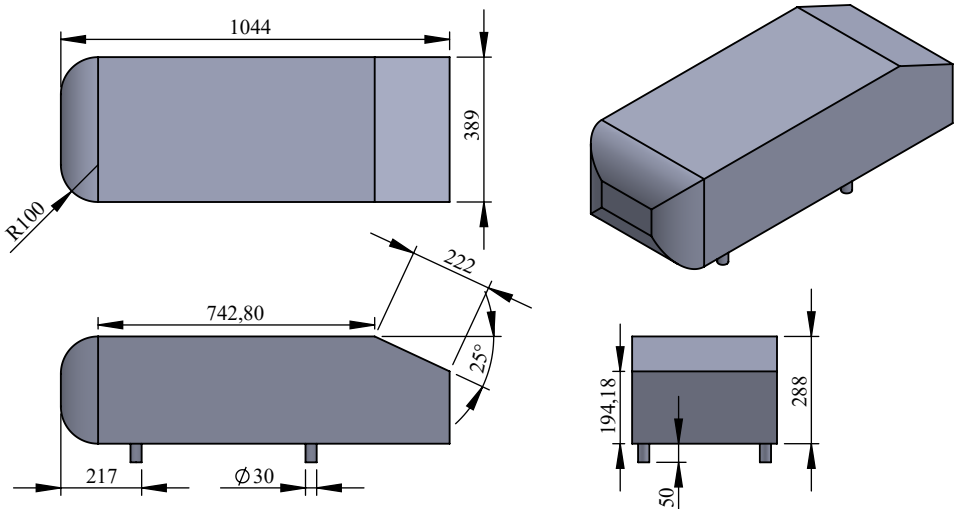

Figure 1. Ahmed's body reference geometry, main dimensions (mm) for slant angle of 25.0°

Despite the considerable deviation of this geometry from the usual vehicles, this generic geometry represents the basic aerodynamic properties of a real vehicle, especially at the rear (Meile *et al.*, 2011)

Table 1. Ahmed's body reference geometry, main dimensions for slant angle of 25.0°

Length (mm)	Height (mm)	Width (mm)	Front Area (mm^2)	Height from floor (mm)
1044.00	288.00	389.00	113.53	50.00

The computational domain is one of the most important aspects to be carefully designed, because inside is where the

mesh (control volumes or elements) is created and also where the conservation equations are solved, (Govardhana and Reddy, 2014). The fluid domain of this work was created in the ANSYS^{TM} Design Modeler tool using the enclosure option. A rectangular section was designed and the used as the test section of a virtual wind tunnel. On the other hand, taking advantage of the symmetry of Ahmed's body reference geometry, only the half of the body was used to develop the simulations, (Hetawal *et al.*, 2014). Following the recommendation given by Agarwal (2013), the frontal distance conformed from the velocity inlet to the frontal area of Ahmed's geometry has three times the length of the geometry (3L = 3132 mm). This distance allows the development of the flow before it reach the geometry surface. Figure 2(a) shows the main dimensions of the virtual test section of the wind tunnel.

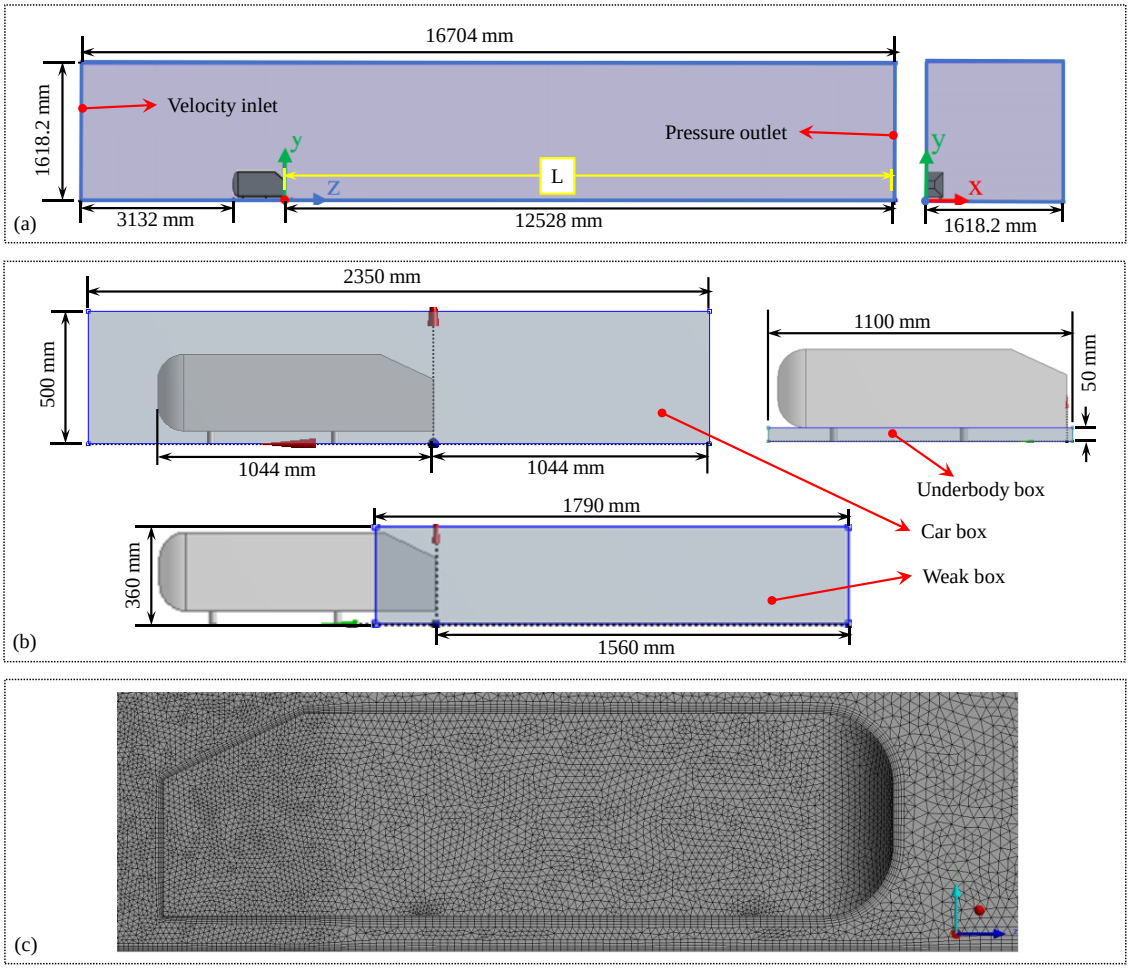

Figure 2. (a) Wind tunnel virtual test section, (b) Influence volumes used in this work, (c) Mesh details around the Ahmed body reference geometry

The blockage ratio is defined as the ratio of the cross-sectional area of the geometry to the cross-sectional area of the computational domain, see right side of figure 2(a). Therefore, a large blockage ratio value means that the walls of the virtual wind tunnel section can increase the pressure on the Ahmed's body reference geometry, which changes the behavior of the flow around the surfaces (Mokhtar *et al.*, 2016). In order to ensure that the blockage ratio in the present study did not have any influence on the results, the values of some numerical studies using the Ahmed's geometry presented below were considered to define the value of the blockage ratio in this work. Bayraktar and Bayraktar (2006) conducted a research on the Ahmed's geometry, with a blockage ratio of 3.5%. This value did not show any effect of pressure on the surfaces. Altinisik *et al.* (2015) also observed through contours of pressure and velocity of a scale car, small pressure changes between the blocking ratio equal to 0% and 5%. On the other hand, these effects increased for blockage ratios between 5% and 20%. For this reason, the value of the blockage ratio in this study was determined as 2.2%. This value was selected because it has no interference on the geometry.

2.1 Experimental data from literature

The airflow around Ahmed body reference geometry was exhaustively analyzed in an experimental study called flow around a simplified body (Ahmed body). Conducted by Lienhart *et al.* (2002), which is part of the European Research

Community's Classic Collection on Flow, Turbulence and Combustion - ERCOFTAC (UMIST, 1995). The slant rear angles of 25.0° and 35.0° were analyzed, because they are on both sides of the critical 30.0° angle, in which the greatest drag is generated. The experiments were carried out in the low-speed wind tunnel (LSTM), with a cross-section of 1.87 x 1.4 m^2. The dimensions of the tested body used were the original ones established by Ahmed (1984). The Reynolds number was Re = 768.000, based on the height of the geometry H = 288 mm and the velocity U_b = 40 m/s. The LSTM can generate flow rates from 3 to 55 m/s with a low average turbulence intensity of less than 0.25%. The instruments used to measure the flow around the geometry were: a computer-based feedback control system to ensure constancy of test section velocity and air temperature; a hot wire was used to measure velocity in non-permanent flows (turbulent), and Laser Doppler Anemometry (LDA) for flow visualization. Six measurements were made at the top and side, and five at the bottom of the geometry. In addition, the three components of mean velocity (RMS) were measured, through 7.500 discrete measurement positions located in 13 planes, approximately 40.000 measurements were made with a time of almost 5 minutes in each location to obtain reliable results. In addition, some measurement planes were created to observe the velocity field around the geometry and the area of the wind tunnel. Inside the wake of the Ahmed's geometry, there is a high turbulence intensity and average velocities can approach to zero. Therefore, the uncertainty of the results obtained is only about 1.5%. For more information, this study can be found in the (ERCOFTAC) database, where is presented more results such as pressure measurements on the back area of the geometry, flow measurements on the inclined surface and in the wake, showing in detail the points of separation and recirculation. This quantitative and qualitative information serves as a basis for developing, testing and validating aerodynamic studies. For this reason, this research, among other experimental investigations were invoked to validate the results obtained through the numerical simulations of this study.

2.2 Geometry, mesh parameters and mesh independence test

Along the mesh generation, some strategies were performed in order to increase the mesh quality. For this reason, a hybrid mesh was created, which is conformed by hexahedral elements around the surface of the Ahmed body reference geometry and tetrahedral elements in the remaining parts of the computational domain. Through the technique of local refinements within the mesh, refinements were applied to the elements of the entire geometry, which were divided in two types. Firstly, an element size of 10 mm was applied to each one of the faces of the geometry excluding stilts and second, an element size of 2 mm was applied to each one of the four body-supporting legs. Using the refinement strategy based on volumes of influence, which allows to combine different types of elements within a mesh and directly control the size of the cells, three volumes were introduced as shown in Figure 2(b). The first, the Carbox influence geometry, was located in the entire region surrounding the surfaces of the Ahmed's geometry; the second one, was the underbody box, which was positioned between the road and the region of the ground surface of the geometry, to obtain the main features around the stilts and the rear area, shown at the top right of Figure 2(b); and to capture accurately the fluid field in the wake area a third influence geometry called wake-box, was placed before the inclined surface in order to capture the separation and recirculation area properly, as shown at the bottom of Figure 2(b). This strategy was essential, because it ensures that the mesh will properly resolve the effects of velocity, pressure and boundary layer around the surface. Therefore, the element size values for the influence volumes were defined through a mesh independence study, which will be covered in a better way in the following sections.

2.3 Simulation set-up

The air velocity of 40 m/s was selected for all the numerical simulations in this work, which means that this velocity is below Mach 0.3, consequently the effects of compressibility can be ignored (Çengel and Cimbala, 2018). Therefore, the selected solver was pressure-based this is the best choose for incompressible flows at low velocity and its capacity has been extended to operate at low Mach numbers, (Mangani *et al.*, 2016). Nowadays, through computational fluid dynamics software, the analysis of laminar flows can be easily performed. Conversely, it happens for the simulation of turbulent flows, since there is no an universal turbulence model. Therefore, it is necessary to invoked a turbulence model that contains the fluid dynamic properties of the simulation to be studied, (Çengel and Cimbala, 2018). For this reason, the simulations of this project were developed with four turbulence models: κ - ε Realizable, κ - ε RNE, κ - ω Standard, and RSM. The first three models have two transport equations, while the last one has seven transport equations. Each one of these models have different configurations to predict the behavior of the flows. For example, the Realizable κ - ε turbulence model, is one of the most used for external aerodynamic simulations, since it allows to know with precision the points of separation of the fluid around the surface. It also solves the boundary layer, the adverse pressure gradients and rotational fluids (vortices) (Altinisik *et al.*, 2015), in industrial applications this model has shown reliable results, with an accuracy between 2-5% (Lanfrit, 2005). While, the RNG κ - ε: has additional terms for the dissipation equation ε, which improves the accuracy of rapidly tense flows, swirling flows, and the ability to handle low Reynolds numbers, (ANSYS, 2018). On the other hand, κ - ω turbulence model belongs to the model of two equations, one for turbulent kinetic energy κ and another for the specific dissipation rate of turbulent energy ω, which captures free shear flows and flow recirculation on flat plates, and the RSM, being currently the most elaborate turbulence model, because it

solves three-dimensional cases with 7 transport equations. Showing high accuracy to capture streamlines curvature, eddy rotation and rapid changes in deformation velocity. Figure 3 shows the boundary conditions used in this work for all runs, which represent the interaction of the walls with the body, playing an important role in the output of the results. At the same time, it can be imposed the initializations conditions related to the physics of the simulation, being a fundamental parameter representing real life conditions within a numerical simulation (Tu *et al.*, 2018).

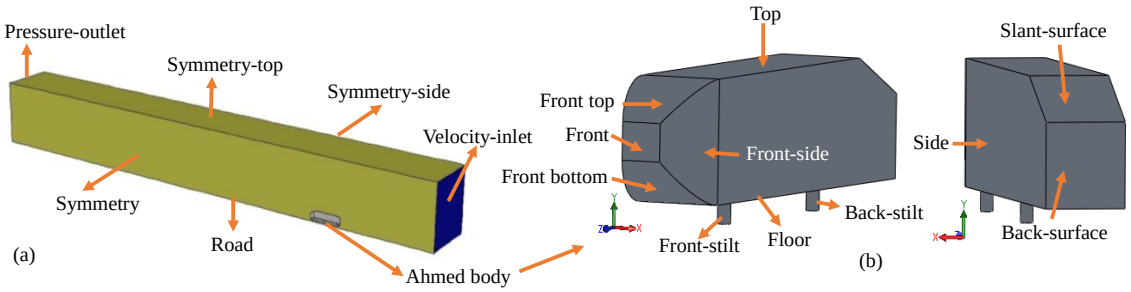

Figure 3. Boundary conditions - Simulation set-up: (a) virtual wind tunnel test section, (b) Ahmed's body surface names

Through the velocity inlet boundary condition the value of the incoming flow velocity was introduced for the development of the simulations, which is equal to 40 m/s (144 km/h). Additionally, in this boundary condition was defined the value of the turbulent intensity, also known as the turbulence level, which is defined by the root mean square of the turbulent velocity over the mean velocity of the flow. Therefore, following the recommendations given at CFD-online. (2008) and ANSYS-FLUENT (2014), the selected value was 1%. On the other hand, the value of the turbulent viscosity ratio was also configured, which determines the level of turbulence viscosity that the flow will have, the value of 10 was selected following the recommendations given by ANSYS-FLUENT (2014). The pressure-outlet boundary condition was selected to allow the flow out of the computational domain in a manner similar to the exhaust duct of a car at atmospheric pressure, while the outer limits of the virtual wind tunnel were defined as symmetry boundary conditions, such as: symmetry-top, symmetry side and symmetry, (Çengel and Cimbala, 2018). Because, this boundary condition ensures that the flow will no cross the walls of the computational domain (Bayraktar and Bayraktar, 2006), and finally through the wall condition, the road and vehicle surfaces were selected as non-slip walls.

3. RESULTS AND DISCUSSION

For all simulations the solution was considered as "converged" when the residual of all the transport variables were below $1x10^{-4}$. Two numerical independence tests where performed in order to warrant that numerical results have not dependency on computational domain length and on mesh size.

3.1 Computational domain length and Mesh size independence tests

The distance [L] from the rear surface of the Ahmed body reference geometry to the exit of the numerical wind tunnel was defined for domain length independency analysis (Figure 2(a)). To develop this study, the rear length [L] was varied between 0.5 L and 14 L, where L denotes the total length of the Ahmed body geometry (1044 mm), as shown in Table 2. On the other hand, the same dimensions and refinement parameters were maintained for the underbody-box and car-box influence volumes (Figure 2(b)), while the dimensions and refinement parameters of the wake-box were varied proportionally with the back length of the computational domain, this means that the size of this volume of influence was varied as the study of independence of the length of the computational domain was executed, once this length was defined, the study of mesh independence test was carried out. The drag coefficient c_D was selected to analyze the convergence and independence criteria. Table 2 shows difference percentage between the drag coefficients of the simulations as well as the value of the back length of the computational domain, the length of the wake box and the total number of elements for each case are presented. Table 2 also shows results that drag coefficient (c_D) after the simulation of 4L, had a convergence tendency. However, for the value of 12L a higher value was observed, compared to the previous ones. One of the hypotheses to explain this small discrepancy is the low number of elements used for this configuration being equal to 2596832. Therefore, to determine and analyze this behavior, the mesh independence study was executed on the computational domain length of 12L. For the velocity range on automotive industry (passengers cars), the Ahmed body reference geometry may present a large wake region. Thus, it is important to use an adequate element size to accurately resolve the boundary layer, vortices and recirculation area. Unfortunately, each mesh generated can give different results. For this reason, a mesh independence study was carried out with different refinements to ensure that the results of the simulations were independent of the number of elements of the mesh, Table 2 also shows the results. Many hours of simulations were necessary to perform this analysis, but it was assured that the results obtained were independent of the

number of elements. The mesh refinement was made by means of influence volumes (boxes), which allow to increase the number of elements in the areas of greater interest. Consequently, to determine this analysis, the κ - ε was selected, following the recommendations several works available in the literature Govardhana and Reddy (2014); Bayraktar and Bayraktar (2006); Lanfrit (2005) and references therein).

Table 2. Independence tests performed in this work

Computational domain length independence test					**Mesh size independence test**		
Rear length	**Length of the weak box (mm)**	**Number of elements**	$\mathbf{c}_D$	$\Delta\,\mathbf{c}_D$ **(%)**	**Number of elements**	$\mathbf{c}_D$	**Diff (%)**
0.5·L	65	1300691	0.31400	-	202711	0.3469	-
2·L	260	1605143	0.29021	7.57718	544067	0.2979	14.116
4·L	520	1766504	0.29059	-0.13327	880479	0.2948	1.047
6·L	780	1937307	0.28972	0.30192	1565698	0.2915	1.111
8·L	1040	2089410	0.28965	0.02332	2596832	0.2902	0.433
10·L	1300	2330904	0.28938	0.09160	3997816	0.2891	0.403
12·L	1560	2596832	0.29024	-0.29664	5421579	0.2872	0.664
14·L	1820	2868079	0.28898	0.43502	8830146	0.2869	0.095

Figure 4 shows the trend of both the independence test performed in this work. Please note that on Figure 4(a) the x-axis represent the rear length [L] in meters and Figure 4(b) the x-axis represent the number of elements of each mesh progressively reducing the mesh size. After the fourth case of refinement, the difference between the c_D values shown a percentage lower than 1%, reaching this state can be considered that the mesh will reproduce results with no dependency of the mesh size. Since the value of 5421579 elements showed a difference of only 0.664% with respect to the previous value, it was selected for all numerical simulations, in order to compare numerical results of this work to experimental data available at literature. On the other hand, to achieve this number of elements, it was defined a specific value of the size of the elements for each one of the influence volumes (see Figure 2(b)): the car-box has an element size of 15 mm, the underbody-box has a size of 10 mm and the wake-box has an element size of 7 mm . Figure 2(c) shows details of the mesh refinement around the Ahmed body.

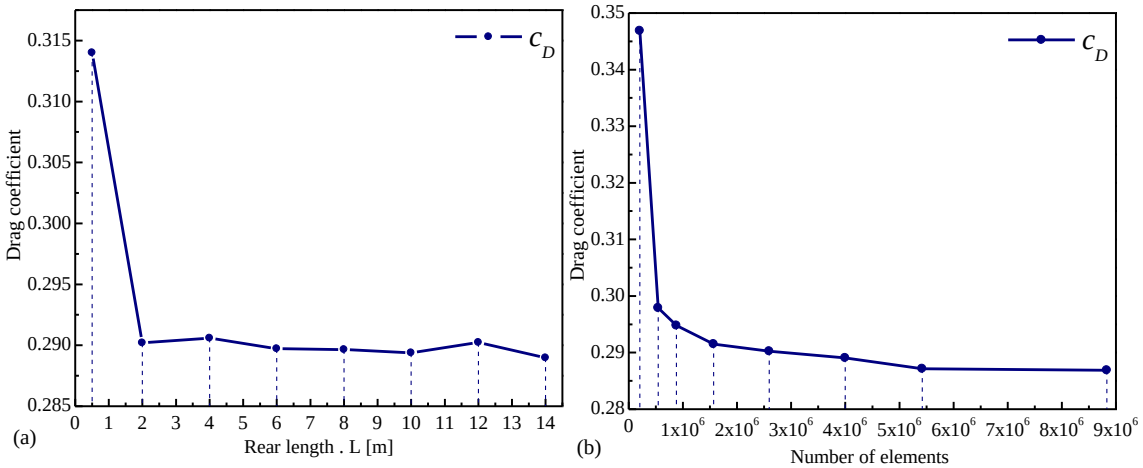

Figure 4. Independence tests: (a) length of computational domain, (b) mesh size as function of elements number - (All numerical simulations performed using κ - ε Realizable turbulence model)

To guarantee the mesh quality some statistical aspects were observed: skewness, orthogonality and aspect ratio. The first one determines the proportion of a face or cell of an element to be ideal (ANSYS, 2018), the mesh used in this work has a skewness with an average value 0.205 (the ideal being equal to 0.0). The orthogonality shown an average value of 0.793 (the ideal being equal to 1.0). The aspect ratio is the measure of the deviation of a mesh element from having all sides of equal length, in this work the average value was 1.92 (the ideal being equal to 1.0). The non-dimensional parameter for check the adequate height of the elements related to the boundary layer flow solution, y^+, determines the height of the boundary layer from a surface to the first mesh node. Which means that this value has to remain in an adequate range to capture the development of the boundary layer. Large y^+ values may be outside the boundary layer and too small values are not recommended, because the height of the elements can be located in the viscous sublayer. On the other hand, the value of y^+ is dependent on the local velocity of the fluid around the geometry. Therefore, it is only

possible to know the exact value of this parameter after the simulation finished. For this reason, this value is determined at the post-processing stage (Leap-CFD., 2012). It is generally recommended that this value be in the range of $30 < y^+ < 300$ for a turbulence model with wall functions (ANSYS-FLUENT, 2014) Figure 5(c) shows the y^+ values around the Ahmed body reference geometry, it is observed that the values obtained are in the recommended range.

3.2 Drag and lift coefficients

This section is divided into two stages. In the first stage it presents the value of drag and lift coefficients contribution of each one of the surfaces of the Ahmed's geometry, and in the second stage it presents a comparison of the drag coefficient obtained in the simulations with a drag coefficient obtained experimentally. To properly capture the external aerodynamics over the geometry in addition to performed simulations with the κ - ε Realizable, three additional turbulence models were selected, such as: κ - ε RNG, κ - ω Standard and RSM. On the other hand, to properly analyze the results of the simulations, Table 3 show the value of the drag and lift coefficients for each one of the surfaces (local contribution) of the Ahmed's geometry, shown in the Figure 3(b), and the total value of the drag and lift coefficient obtained for all turbulence models used in this work. In order to make a comparison between the values of drag obtained in the simulations is introduced the experimental work elaborated by Meile *et al.* (2016). Using the original dimensions the model was build with wood materials, the model has a blocking ratio of 3.8%. The analyses were performed with a velocity of 40 m/s and the data acquisition was obtained by means of pressure taps positioned around the inclined back to capture the velocity, the aerodynamic forces on the body were measured with a six components platform balance, a total drag coefficient equal to 0.29883 was determined with only a calibration uncertainty of $\pm$0.5% of the measured value.

Table 3. Drag and lift coefficients predicted by using the four turbulence models in this work

Surface name	κ - ε **Realizable**		κ - ε **RNG**		κ - ω **Standard**		**RSM**	
	c_D	c_L	c_D	c_L	c_D	c_L	c_D	c_L
Side	0.01555	0.00027	0.01467	0.00020	0.01726	0.00025	0.01613	0.00024
Front side	-0.07671	0.00032	-0.07645	0.00030	-0.07692	0.00030	-0.08221	0.00018
Front	0.13975	0.00007	0.13963	0.00007	0.13944	0.00004	0.13805	0.00003
Front top	-0.06180	0.26360	-0.06154	0.26271	-0.06288	0.26419	-0.06537	0.26568
Front bottom	0.04257	-0.14593	0.04349	-0.14337	0.04879	-0.13272	0.04455	-0.14278
Floor	0.01064	-0.63132	0.00958	-0.63446	0.01150	-0.62086	0.01110	-0.66381
Top	0.00940	0.60350	0.00883	0.60515	0.01000	0.60150	0.00939	0.61819
Slant surface	0.12890	0.27244	0.12743	0.26957	0.12485	0.26289	0.13055	0.27517
Back surface	0.06062	0.00003	0.05694	0.00002	0.04838	0.00006	0.06199	0.00001
Front stilt	0.00932	-0.00002	0.00912	-0.00006	0.01322	0.00004	0.00958	-0.00004
Back stilt	0.00889	-0.00002	0.00829	-0.00004	0.01029	-0.00005	0.00617	0.00002
Total	0.28715	0.36293	0.27998	0.36008	0.28393	0.37564	0.27991	0.35287

Table 4 shows the percentage difference between the experimental to numerical results. It can be observed that the κ - ε realizable turbulence model has the lowest difference to predict the value experimentally, with only 3.90% of difference. At the same time it was determined that the other turbulence models testes in this work also adequately captured the total drag value, the maximum difference was of 6.33%. This indicates that the mesh quality as well as the set-up used in this work are adequate to determine the external aerodynamics over the surfaces of the geometry in terms of drag. To validate the lift, the experimental research conducted by Meile *et al.* (2011) was used to validate the lift coefficients. In this investigation the generic Ahmed body was used with the original dimensions, with an angle of inclination of 25° and air velocity of 40 m/s. The value of the lift coefficient obtained was equal to 0.345. Table 4 presents the results of the lift coefficient for the four turbulence models and the percentage difference against the experimental value. The smallest difference obtained was 2.28%. While the largest difference was 8.88%.

Table 4. Numerical vrs. experimental data of drag (Meile *et al.*, 2016) and lift (Meile *et al.*, 2011) coefficients

Turbulence model	c_D **- sim**	c_D **- exp. (0.298)**	c_L **- sim**	c_L **- exp. (0.345)**
		Diff (%)		Diff (%)
κ - ε **Realizable**	0.28715	3.90858	0.3629	5.1983
κ - ε **RNG**	0.27998	6.30686	0.3601	4.3717
κ - ω **Standard**	0.28393	4.98456	0.3756	8.8819
RSM	0.27991	6.33135	0.3529	2.2825

This means that while some turbulence models are suitable for capturing the drag, others can better capture the lift. Apart from this, the positive value of the lift coefficient for the 25° slant angle indicates that the flow between the ground

(road) and the Ahmed body floor has low velocity, as a result there is a higher pressure at the bottom than at the top, which generates a positive lift force. The realizable κ - ε model resolves in a better way the turbulent viscosity, at the same time it has new transport equations for the dissipation rate, and satisfies certain mathematical constraints on the Reynols stresses, in agreement with the physics of turbulent flows. A benefit of the model is that it more accurately predicts the spreading rate of planar and round surfaces, and provides a superior performance for flows involving recirculation, boundary layers under strong adverse pressure gradients, separation, and rotation. For this reason it was observed that the realizable κ - ε model predicts the drag coefficient (c_D) accurately ANSYS (2018). On the other hand, the Reynolds Stress Model (RSM) is one of the most elaborate types of turbulence models, solving seven transport equations for 3D cases. It was also the most computationally time consuming. Thanks to its great ability to predict more accurately the different pressure gradients around flat surfaces and streamlines, (ANSYS, 2018), it was observed that for Ahmed's reference body, this turbulence model showed greater proximity to the experimentally calculated lift value.

3.3 Flow field

Hucho (1998) shows, schematically, the flow field around the Ahmed body reference geometry. The numerical simulations performed in this work were able to capture the main vortex (shapes) for 25° slant angle as observed comparing Figures 5 (a) and (b). The planes P1, P2, P3 and P4 in Figure 5(d) also shows the fluid evolution in the wake region and will be used for data analysis on Figure 6.

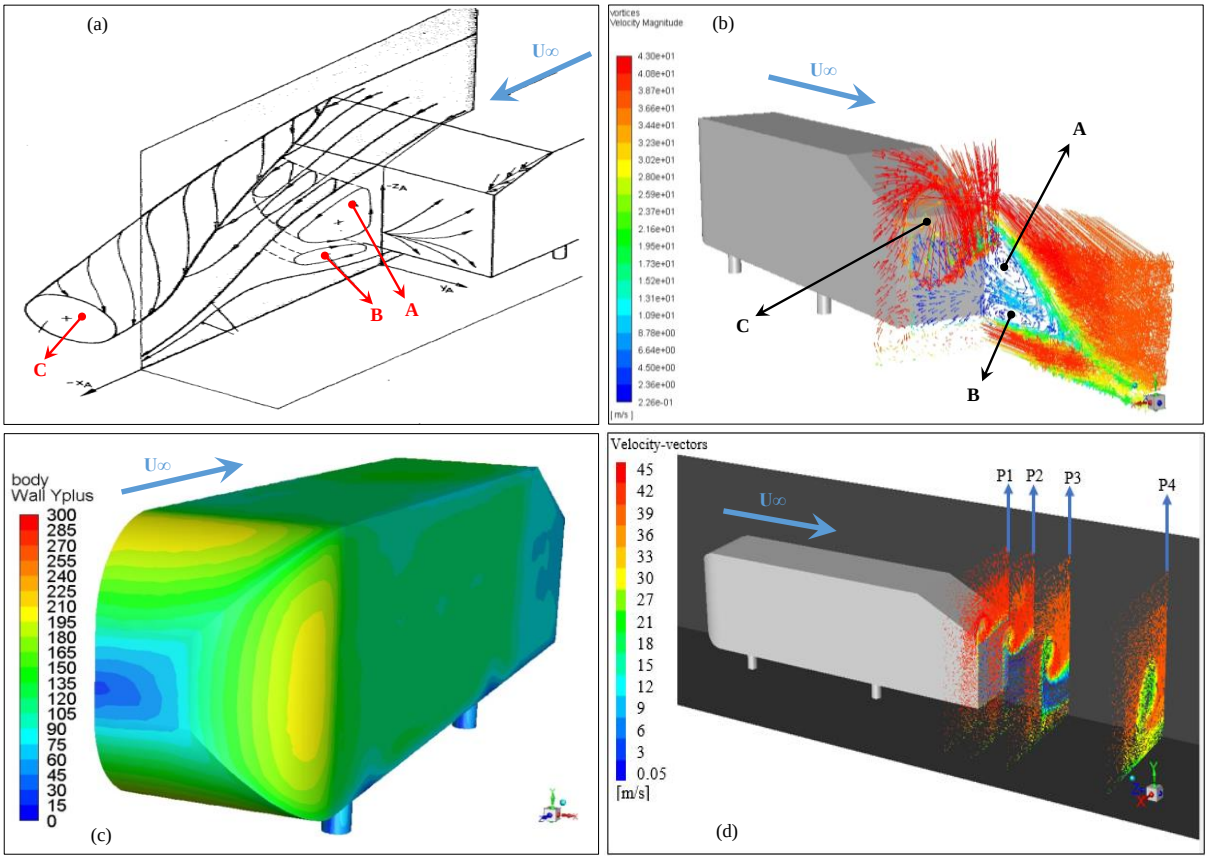

Figure 5. (a) Vortex around the slant and wake region. Adapted from Hucho (1998) (b) Vortex around the slant and wake region - this work - (κ - ε Realizable turbulence model) (c) y^+ values around the Ahmed body (κ - ε Realizable turbulence model) (d) Velocity vector planes in the wake region - this work - (κ - ε Realizable turbulence model)

Figure 6 compare the numerical and experimental behavior of the fluid field in the wake region for the four planes of Figure 5(d). It can be observed a good agreement in the fluid field shape as well as in the flow evolution along the wake region. Comparing Figures 5(d) and 6 it is possible to see the flow evolution in the air flow direction thorough the wake.

With the intention of validating the velocity field around the surfaces and in the wake region, the experimental research developed by Lienhart *et al.* (2002) was used. In that work, eight velocity lines were created on the entire computational domain, of which five velocity lines are over the surface of the geometry at coordinates z = 178 mm, z = 138 mm, z = 88 mm, z = 38 mm and z = 0 mm and three velocity lines in the region of the wake, at points z = –80 mm, z = –200 mm and z = –500 mm. These lines are located at the coordinate x = 80 mm from the symmetry plane (x = 0.0). In order to make

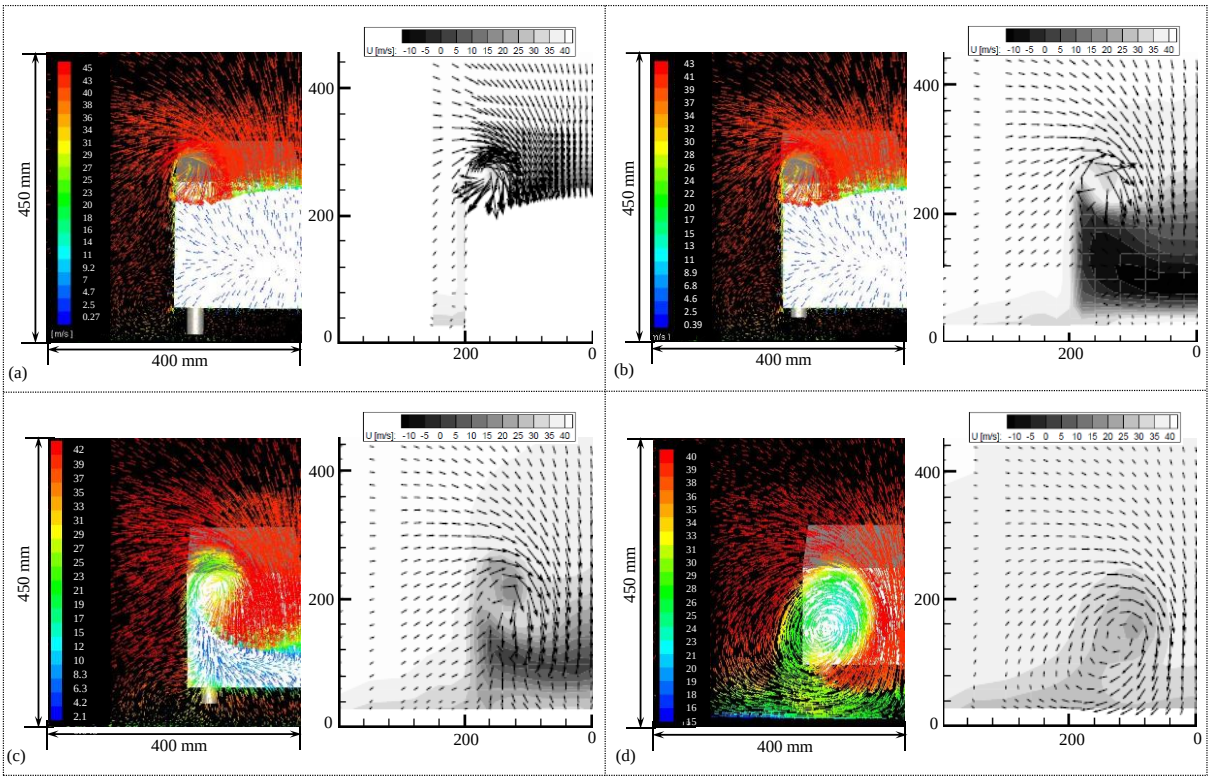

Figure 6. Numerical vs experimental (Lienhart *et al.*, 2002) velocity vectors plots at planes: (a) P1, z = 0.0 mm, (b) P2, z = –80 mm, (c) P3, z = –200 mm and, (d) P4, z = –500mm

a comparison of the velocity distribution in these coordinates, the same lines were created from the numerical results of this work and plotted as shown in Figure 7, where the colored lines represent the numerical results and the colored dots represent the experimental results.

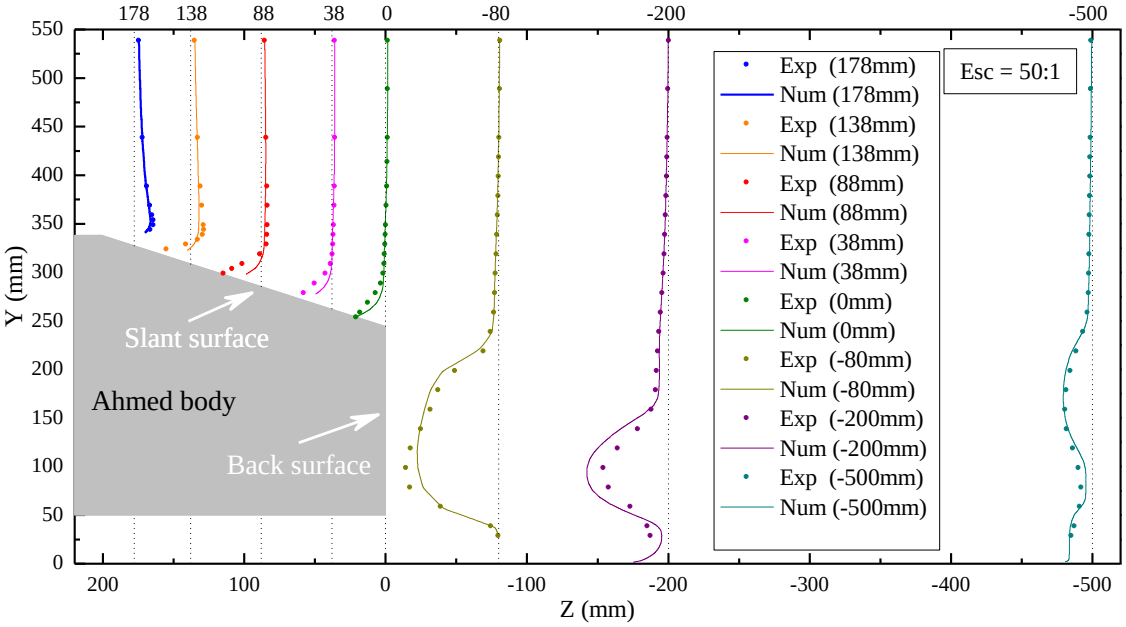

Figure 7. Velocity distribution at slant surface and wake region of the Ahmed body reference geometry - (κ - ε Realizable turbulence model)

4. CONCLUSSION

Through CFD was possible to simulate the flow field around the Ahmed body reference geometry for 25° slant angle in the rear surface. The main conclussions of this work are listed as folows:

- Relevant data related to drag and lift was obtained and well compared to experimental results previously published in the literature, the numerical procedures as set-up, computational domain length and mesh size were then correctly chosen and the small differences for drag and lift coefficient found in this work can support that.

- Numerical results shows that the realizable κ - ε turbulence model well approximates the drag with 3.9% difference to experimental results and the Reynolds Stress Model better fits the lift with 2.8% difference to experimental results.

- The external aerodynamics of the Ahmed body reference geometry was understood and analyzed, where important flow behaviors were observed, such as: the vortices generated on the sides and in the rear area, which depend largely on the rear slant angle; an area of recirculation over the inclined area of the surface, which is generated by the separation of the flow; the effects of turbulence on the rear of the reference body, which can be felt more than half a meter away; and the velocity contours on the geometry and in the region of the wake.

- Velocity profiles on the wake region where then plotted and compared to experimental results obtaining good agreement. In function of the numerical to experimental agreement, it was possible to assess the relevancy in the use of CFD for aerodynamics analysis when adequate chooses are done in set-up and mesh options

- All the methods used in this work can be extrapolated to real automotive geometries in order to, for example, reduce the drag or improve the lift of vehicles, which is directly proportional to fuel consumption.

5. ACKNOWLEDGEMENTS

The authors likes to acknowledge to the Prof. Modesto Hurtado Ferrer, Dr. Eng, at CTJ/UFSC Joinville for the use of ANSYS-FLUENT in this work. The support of UFSC Joinville TI team is also highly appreciated. The financial help for the stay at LABMCI/CTJ/UFSC from the *Oficina de Relaciones Internacionales - ORI* at Francisco de Paula Santander University is also appreciated.

6. REFERENCES

Agarwal, R., 2013. "Sustainable Ground Transportation: Technologies, Challenges and Opportunities". Vol. ASME 2013 7th International Conference on Energy Sustainability of *Energy Sustainability*. doi:10.1115/ES2013-18028.

Ahmed, S., Ramm, G. and Faltin, G., 1984. "Some salient features of the time-averaged ground vehicle wake". In *SAE International Congress and Exposition*. SAE International. ISSN 0148-7191. doi:https://doi.org/10.4271/840300.

Altinisik, A., Kutukceken, E. and Umur, H., 2015. "Experimental and Numerical Aerodynamic Analysis of a Passenger Car: Influence of the Blockage Ratio on Drag Coefficient". *Journal of Fluids Engineering*, Vol. 137, No. 8. ISSN 0098-2202. doi:10.1115/1.4030183.

ANSYS, 2018. "Ansys documentation - help." ANSYS-FLUENT 2018 DOC. <https://www.ansys.com/products/fluids/ansys-fluent>.

ANSYS-FLUENT, 2014. "Ansys fluent lecture 7: Turbulence modeling - introduction to ansys fluent 15.0 release". ANSYS Confidential.

Bayraktar, I. and Bayraktar, T., 2006. "Guidelines for cfd simulations of ground vehicle aerodynamics". In *SAE 2006 Commercial Vehicle Engineering Congress Exhibition*. SAE International. ISSN 0148-7191. doi:https://doi.org/10.4271/2006-01-3544.

Çengel, Y. and Cimbala, J., 2018. *Fluid Mechanics: Fundamentals and Applications.* McGraw-Hill Education, New York, 4th edition.

CFD-online., 2008. "Eddy viscosity ratio". CFD online. <https://www.cfd-online.com>.

Govardhana, M. and Reddy, V., 2014. "Estimation of drag and lift on ahmed body using cfd analysis". *International Journal of Advanced and Innovative Research*, Vol. 3, No. 52, pp. 2278–7844.

Guilmineau, E., 2018. "Effects of rear slant angles on the flow characteristics of the ahmed body by iddes simulations". In *SAE Technical Paper*. SAE International, 2018-01-0720. URL `https://doi.org/10.4271/2018-01-0720`.

Hetawal, S., Gophane, M., Ajay, B. and Mukkamala, Y., 2014. "Aerodynamic study of formula sae car". *Procedia Engineering*, Vol. 97, pp. 1198–1207. ISSN 1877-7058. doi:https://doi.org/10.1016/j.proeng.2014.12.398. 12th Global Congress on Manufacturing and Management GCMM - 2014.

Hucho, W.H., 1998. *Aerodynamics of Road Vehicles: From Fluid Mechanics to Vehicle Engineering*. SAE, 4th edition.

Lanfrit, M., 2005. "Best practice guidelines for handling automotive external aerodynamics with fluent". FLUENT Deutschland GmbH.

Leap-CFD., 2012. "Wall functiona and y^+ requirements". Leap CFD June 25. <https://www.computationalfluiddynamics.com.au/tips-tricks-turbulence-wall-functions-and-y-requirements/>.

Lienhart, H., Stoots, C. and Becker, S., 2002. *Flow and Turbulence Structures in the Wake of a Simplified Car Model (Ahmed Modell).* Springer, Heidelberg. In: Wagner S., Rist U., Heinemann HJ., Hilbig R. (eds) New Results in Numerical and Experimental Fluid Mechanics III. Notes on Numerical Fluid Mechanics (NNFM), vol 77.

Mangani, L., Sanz, W. and Darwish, M., 2016. "Comparing the performance and accuracy of a pressure based and a density-based coupled solver". In *16th International Symposium on Transport Phenomena and Dynamics of Rotating Machinery*. Honolulu, United States. URL `https://hal.archives-ouvertes.fr/hal-01894391`.

Meile, W., Brenn, G., Reppenhagen, A. and Fuchs, A., 2011. "Experiments and numerical simulations on the aerodynamics of the ahmed body". *CFD Letters*, Vol. 3, No. 1, pp. 32–39.

Meile, W., Ladinek, T., Brenn, G., Reppenhagen, A. and Fuchs, A., 2016. "Non-symmetric bi-stable flow around the ahmed body". *International Journal of Heat and Fluid Flow*, Vol. 57, pp. 34 – 47. ISSN 0142-727X. doi:https://doi.org/10.1016/j.ijheatfluidflow.2015.11.002.

Mokhtar, W., Madagi, C. and Hasan, R., 2016. "Further study of wall interference for high blockage vehicles in closed test section wind tunnels". *International Journal of Modern Engineering Research*, Vol. 6, No. 10, pp. 58–70.

Stone, R. and Ball, J.K., 2004. *Automotive Engineering Fundamentals*. SAE International, Warrendale, Pa.

Tu, J., Yeoh, G. and Liu, C., 2018. *Computational Fluid Dynamics - A Practical Approach.* Butterworth-Heinemann, 50 Hampshire Street, 5th Floor, Cambridge, MA 02139, United States, 3rd edition. ISBN 978-0-08-101127-0.

UMIST, 1995. "European research community on flow, turbulence and combustion database". ERCOFTAC Classic Collection <http://cfd.mace.manchester.ac.uk/ercoftac/>.

7. RESPONSIBILITY NOTICE

The author(s) is (are) solely responsible for the printed material included in this paper.